ARTICLES

Study of Photoinduced Electron Transfer between [60]Fullerene and Proton-Sponge by Laser Flash Photolysis: Addition Effects of Organic Acid

Rumiko Horie,[†] Yasuyuki Araki,[†] Osamu Ito,*[,†] Yangsoo Lee,[‡] Toshikazu Kitagawa,[‡] and Koichi Komatsu[‡]

Institute of Multidisciplinary Research for Advanced Materials, Tohoku University, Katahira, Sendai, 980-8577 Japan, and Institute for Chemical Research, Kyoto University, Uji, Kyoto, 611-0011 Japan

Received: March 10, 2005; In Final Form: April 24, 2005

Photoinduced electron-transfer processes between fullerene (C_{60}) and 1,8-bis(dimethylamino)naphthalene, which is called a proton-sponge (PS), have been investigated by means of laser flash photolysis in the presence and absence of CF_3CO_2H. For a mixture of C_{60} and PS, the transient absorption spectra showed the rise of the C_{60} radical anion with concomitant decay of the C_{60} triplet ($^3C_{60}$*), suggesting that photoinduced intermolecular electron transfer occurs via $^3C_{60}$* in high efficiency in polar solvent. For a covalently bonded C_{60}−PS dyad, photoinduced intramolecular charge-separation process takes place via the excited singlet state of the C_{60} moiety, although charge recombination occurs within 10 ns. For both systems, electron-transfer rates were largely decelerated by addition of a small amount of CF_3CO_2H, leaving the long-lived $^3C_{60}$*. These observations indicate that the energy levels for charge-separated states of the protonated PS and C_{60} become higher than the energy level of the $^3C_{60}$* moiety, showing low donor ability of the protonated PS. Thus, intermolecular electron-transfer process via $^3C_{60}$* for C_{60}−PS mixture and intramolecular charge-separation process via $^1C_{60}$*−PS for C_{60}−PS dyad were successfully controlled by the combination of the light irradiation with a small amount of acid.

Introduction

Fullerene C_{60}, which is a good electron acceptor, has been studied for more than 15 years as a central component of photoinduced electron-transfer systems.[1−4] Recent interests in this field were to control chemically the nature of the electron-donor and electron-acceptor systems for new applications.[5−7] For this aim, research of good electron donors with respect to C_{60} has been continued by precise investigation of electron-transfer kinetics.[1−7] It has been well understood that various aromatic amines work as strong electron donors in photoinduced electron transfer, when C_{60} is mixed with amines in polar solvents.[8−17] When amines with strong basicity are used as donors with respect to photoexcited C_{60}, it would be anticipated that the dynamics of the photoinduced electron transfer can be modified by adding acid to the solution.[18] As such an amine, 1,8-bis(dimethylamino)naphthalene, which is referred to as "proton-sponge" (abbreviated as PS), is one of the candidates, since PS is known as an exceptionally strong base for a tertiary amine.[19−22] Thus, we investigate here the photoinduced electron transfer for the mixture of C_{60} and PS in the presence and absence of a small amount of acid to control the photochemical events.

Furthermore, covalently connected dyads of C_{60} with donor molecules such as aromatic amines have also been extensively synthesized and their photoinduced electron-transfer processes have been studied in relation to the field of material chemistry and biochemistry.[23−29] It is expected to open several applications for high-speed electronic devices, solar cells, medicines, and so on.[4] Lee et al. synthesized a new C_{60}-dyad, in which PS is connected with C_{60} as shown in Chart 1.[30] It is expected that the C_{60}−PS dyad gives a sensitive example to control the

CHART 1: Structures of C_{60}, Proton-Sponge, and C_{60}−Proton-Sponge Dyad

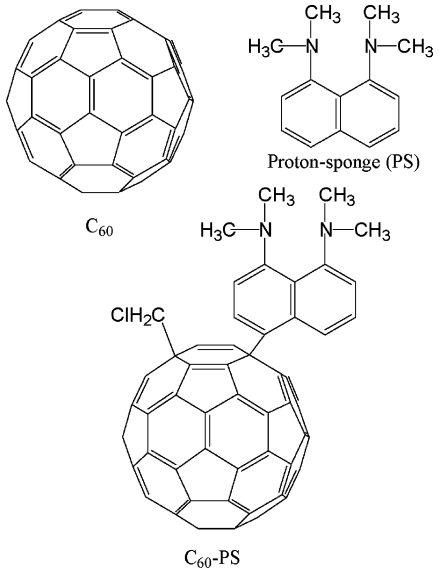

* Author to whom correspondence should be addressed.
[†] Tohoku University.
[‡] Kyoto University.

10.1021/jp051253n CCC: $30.25
Published on Web 06/25/2005

photoinduced charge-separation processes by adding a small amount of acid. In the present study, photoinduced processes of C_{60}−PS dyad have been studied by means of laser flash photolysis in the presence and absence of acid.

Experimental Section

Chemicals. C_{60} (purity = 99.9%), 1,8-bis(dimethylamino)-naphthalene (purity = 99.5%), trifluoroacetic acid (99.5%), and $(n\text{-}C_4H_9)_4NPF_6$ (Fluka puriss quality) were purchased from Term USA, Sigma-Aldrich Inc., Wako Pure Chemical Ind., and Fluka Inc., respectively. The synthesis of C_{60}−PS was reported previously.[30] Solvents such as benzonitrile (PhCN), *o*-dichlorobenzene (*o*-DCB), and toluene were purchased from Wako Pure Chemical Ind. Other chemicals were of the best grade commercially available.

Apparatus. Steady-state absorption and fluorescence spectra in the visible and near-IR regions were measured with a JASCO-V-570DS spectrometer and a Shimadzu RF-5300 PC spectrofluorophotometer equipped with a photomultiplier tube having a high sensitivity in the 700−850 nm region. Nanosecond transient absorption spectra were measured using a second-harmonic generation (SHG; 532 nm) of a Nd:YAG laser (Spectra-Physics, Quanta-Ray GCR-130, fwhm = 6 ns, power < 20 mJ pulse^{-1}) as an excitation source. For the transient absorption spectra in the near-IR region (600−1400 nm) for the time scale up to 2 μs, monitoring light from a pulsed Xe-lamp was detected with a Ge-APD (Hamamatsu Photonics, B2834).[14] For spectra in the visible region (400−700 nm), a Si−PIN photodiode (Hamamatsu Photonics, S1722−02) was used as a detector.[16−18] For long time scale measurements, an InGaAs detector was used to monitor the light from continuous Xe-lamp. All the samples were measured in a quartz cell (1 × 1 cm) and were deaerated by bubbling Ar gas through the solution for 15 min.

Reduction potentials (E_{red}) and oxidation potentials (E_{ox}) were measured by cyclic voltammetry with a potentiostat (BAS CV50W) in a conventional three-electrode cell equipped with Pt-working and counter electrodes with a Ag/Ag^+ reference electrode at scan rate of 100 mV s^{-1}.[31] The E_{red} and E_{ox} were expressed versus ferrocene/ferrocenium (Fc/Fc^+) used as internal reference. In each case, a solution containing 0.2 mM of a sample with 0.05 M $(n\text{-}C_4H_9)_4NPF_6$ was deaerated with Ar gas bubbling before measurements.

Fluorescence lifetimes were measured by a single-photon-counting method using a streakscope (Hamamatsu Photonics, C4334-01) as a detector and the SHG laser light (410 nm) of a Ti:sapphire laser (Spectra-Physics, Tsunami 3950-L2S, fwhm = 1.5 ps) as an excitation source.[32] Fluorescence lifetimes were evaluated with a software attached to the equipment.

Results and Discussion

Mixture Systems. Steady-State Absorption Spectra. Figure 1 shows the UV−vis absorption spectra of C_{60} and PS and their mixture in *o*-DCB. PS shows a sharp peak at 342 nm, which is due to the electronic transition including π-electrons of naphthalene moiety and lone pairs of the N atoms of the amine moieties in PS.[33] C_{60} shows weak broad bands in the 500−600 nm region, in addition to the intense absorption in the wavelength shorter than 400 nm.[1,9,10] The spectrum of the C_{60} and PS mixture solution was almost the sum of the components, suggesting absence of appreciable interaction between C_{60} and PS in the ground state under the present conditions.

To find a possibility to control photoinduced electron-transfer processes of the mixture of C_{60} and PS by the protonation of

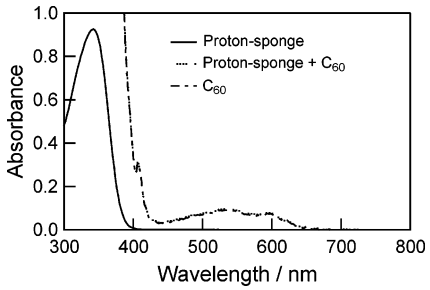

Figure 1. Steady-state absorption spectra of PS (0.1 mM), C_{60} (0.1 mM), and their mixture in *o*-DCB.

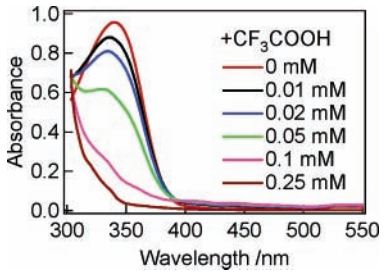

Figure 2. Changes of steady-state absorption spectra of PS (0.1 mM) in PhCN by addition of CF_3CO_2H (0−0.25 mM).

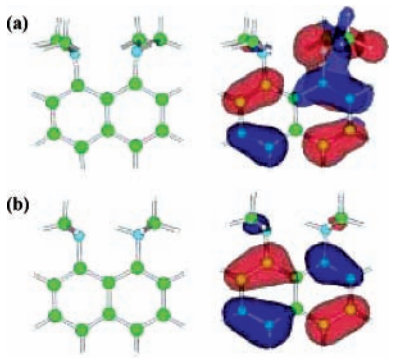

Figure 3. Optimized structures (C: green, N: blue, H: white) and the HOMO; (a) PS and (b) PSH^+.

PS, we first observed the addition effect of CF_3CO_2H on the absorption of PS. As shown in Figure 2, the intensity of the absorption band at 342 nm of PS decreased drastically on addition of a small amount of CF_3CO_2H, reaching finally an absorption similar to that of naphthalene. For example, equimolar CF_3CO_2H completely suppressed the absorption of PS at 342 nm. It is reported that second protonation to PS is difficult in organic solvent because of a steric reason.[34]

Molecular Orbital Calculations. The optimized structure of PS was calculated by Gaussian 98 at B3LYP/3-21G level. In Figure 3a, optimized structures and the HOMO are shown. Two dimethyl groups attached to the N atoms at the 1,8-position are oriented toward opposite directions to minimize the steric crowding of the dimethyl groups.[35] The electron density of the HOMO of PS is localized mainly on one of the N atoms and the whole naphthalene moiety. The optimized structure of protonated PS (PSH^+) is shown in Figure 3b, in which the structure is depicted to show the protonated proton clearly; thus, two backside dimethyl groups seem to be hidden by the front ones. The added proton is connected with one of the N atoms, decreasing drastically the electron density of the protonated N atom, which reduces the electron-donor ability.

Electrochemistry. From the cyclic voltammograms of C_{60} and PS measured in PhCN, the E_{red} was evaluated to be −0.94 versus Fc/Fc^+ from the reversible peak; the oxidation shows an

TABLE 1: Free-Energy Change (ΔG_{et}^0), Quench Rate Constants (k_q), Quantum Yields (Φ_{et}), and Values for Electron Transfer (k_{et}) via $^3C_{60}$* and Back-Electron-Transfer Rate Constants (k_{bet})

	E_{diele}[a]	ΔG_{et}^0 [b]/eV	$k_q/M^{-1}s^{-1}$	Φ_{et}	$k_{et}/M^{-1}s^{-1}$	$k_{bet}/M^{-1}s^{-1}$
PhCN	25.2	−0.68	4.4×10^9	0.60	2.6×10^9	1.3×10^{10}
o-DCB	9.9	−0.46	3.9×10^9	0.09	3.4×10^8	2.6×10^{10}
toluene	2.3		7.1×10^9	0.07	5.3×10^8	(8.9×10^8)[c]

[a] Dielectric constant of solvent. [b] $\Delta G_{et}^0 = E_{ox}(PS/PS^{\bullet+}) - E_{red}(C_{60}/C_{60}^{\bullet-}) - E_c - \Delta E_{00}$,[35] in which $E_{ox}(PS/PS^{\bullet+}) = -0.06$ and $E_{red}(C_{60}/C_{60}^{\bullet-}) = -0.94$ vs Fc/Fc^+, and E_c and ΔE_{00} refer to Coulomb[10] term and transition energy = 1.51 eV for $^3C_{60}$*.[10] [c] First-order decay in s^{-1}.

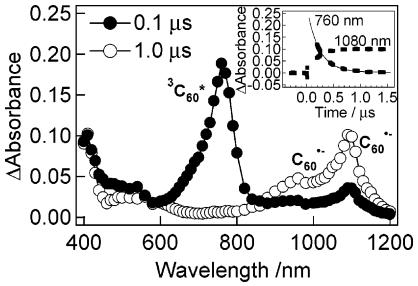

Figure 4. Transient absorption spectra observed by 532-nm laser irradiation of C_{60} (0.1 mM) in the presence of PS (1.0 mM) in PhCN. Inset: Time profiles.

irreversible peak, from which peak potential of oxidation (E_{ox}^p) was evaluated to be at −0.06 V versus Fc/Fc^+. The slightly negative E_{ox} compared with Fc indicates high donor ability of PS. On addition of CF_3CO_2H, the cyclic voltammogram showed irreversible peaks in a more positive region. From these E_{red} and E_{ox}^p values and the excited-state energies of C_{60}, the free-energy changes for electron transfer (ΔG^0_{et}) were evaluated as listed in Table 1, after considering a static term changing with the dielectric constants of solvents.[36]

Nanosecond Transient Absorption Spectra. To investigate the photoinduced intermolecular photoelectron-transfer process between C_{60} and PS, nanosecond transient absorption spectra were measured by laser light excitation of the C_{60} in the presence of PS. Figure 4a shows the transient absorption spectra in PhCN, in which the absorption peak at 760 nm, which appeared immediately after the laser excitation, is identified as the excited triplet state ($^3C_{60}$*).[1−4,9−17] With concomitant decay of the absorption band of $^3C_{60}$* at 760 nm, the absorption peak at 1080 nm appeared at 500 ns, which is assigned to the radical anion of C_{60} ($C_{60}^{\bullet-}$).[9−18] The absorption shoulder at 960 nm is attributed to $C_{60}^{\bullet-}$.[9−18] The absorption bands at 410 and 550 nm are probably due to the radical cation of PS ($PS^{\bullet+}$).[9−18] These observations indicate that electron transfer takes place via $^3C_{60}$* from PS in PhCN. The decay of the absorption peak at 760 nm of $^3C_{60}$* in the inset of Figure 4 can be fitted by a single-exponential function under a pseudo-first-order condition ([PS] ≫ [$^3C_{60}$*]). Similarly, the rise of $C_{60}^{\bullet-}$ at 1080 nm can be fitted with a single-exponential function. From the single-exponential fitting, the first-order rate constant ($k_{first-order}$) can be evaluated for each PS concentration. These $k_{first-order}$ values increase linearly with [PS] as shown in the inset of Figure 5. From the slope of the pseudo-first-order plots, the bimolecular rate constant (k_q) for the quenching of $^3C_{60}$* by PS was obtained. In *o*-DCB and toluene, the k_q values were similarly evaluated as listed in Table 1, in which the k_q values are almost the same as diffusion-controlled limit (k_{diff}).[37] On the other hand, the amount of the rise of $C_{60}^{\bullet-}$ at 1080 nm was quite smaller than those in PhCN.

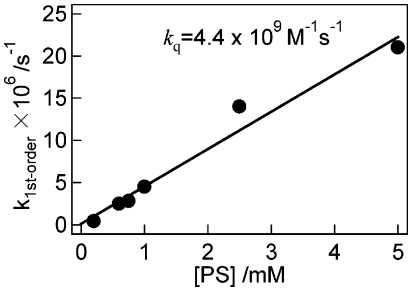

Figure 5. Pseudo-first-order plots for the decay rate ($k_{first-order}$) of $^3C_{60}$* at 760 nm with increase of [PS] in PhCN; slope gives the k_q value.

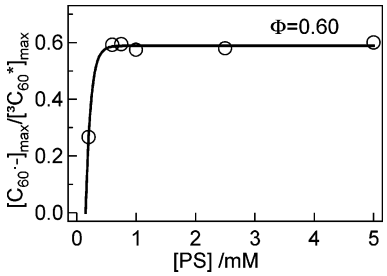

Figure 6. Plots of $[C_{60}^{\bullet-}]_{max}/[^3C_{60}*]_{max}$ against [PS] for electron transfer via $^3C_{60}$* in PhCN.

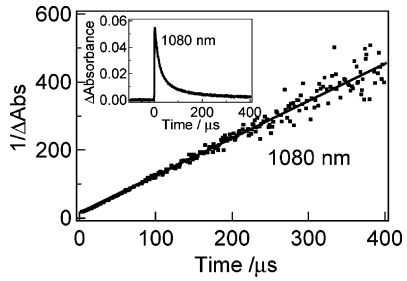

Figure 7. Second-order plot for the decay of $C_{60}^{\bullet-}$ in the presence of equimolar $PS^{\bullet+}$ at 1080 nm in deaerated PhCN. Inset: Observed time profile at 1080 nm.

The ratios of $[C_{60}^{\bullet-}]_{max}/[^3C_{60}*]_{max}$ are plotted against [PS] for electron-transfer process via $^3C_{60}$* from PS in PhCN as shown in Figure 6. The ratios of $[C_{60}^{\bullet-}]_{max}/[^3C_{60}*]_{max}$ saturate at higher PS concentration than 0.5 mM. Usually, the quantum yield (Φ_{et}) of electron transfer via $^3C_{60}$* can be evaluated from the saturated value. Thus, Φ_{et} can be expressed as k_{et}/k_q,[11,38] in which k_{et} refers to electron-transfer rate constant in the process of eq 1. Thus, from the obtained $k_q = 4.4 \times 10^9$ M^{-1} s^{-1} and $\Phi_{et} = 0.60$, k_{et} was evaluated to be 2.6×10^9 M^{-1} s^{-1} in PhCN.

$$^3C_{60}* + PS \xrightarrow{k_{et},\,\Phi_{et}} C_{60}^{\bullet-} + PS^{\bullet+} \qquad (1)$$

In *o*-DCB and toluene, on the other hand, the Φ_{et} values were less than 0.1, suggesting that $^3C_{60}$* is quenched without electron transfer, probably because of the encounter quenching. As shown in Table 1, the k_{et} values in *o*-DCB and toluene are 1 order smaller than that in PhCN, because the Φ_{et} values in *o*-DCB and toluene are small, although the k_q values are close to the k_{diff} value.[37] The k_{et} and Φ_{et} values increase with the negative values of ΔG^0_{et}, while the k_q values are independent from the values of ΔG^0_{et}.

After reaching the maximum, the concentration of $C_{60}^{\bullet-}$ begins decaying in the long time scale measurements as shown in Figure 7. Since the reciprocal of the decay of the transient absorption intensity at 1080 nm was well fitted by a linear line, bimolecular back-electron-transfer process (k_{bet}) takes place

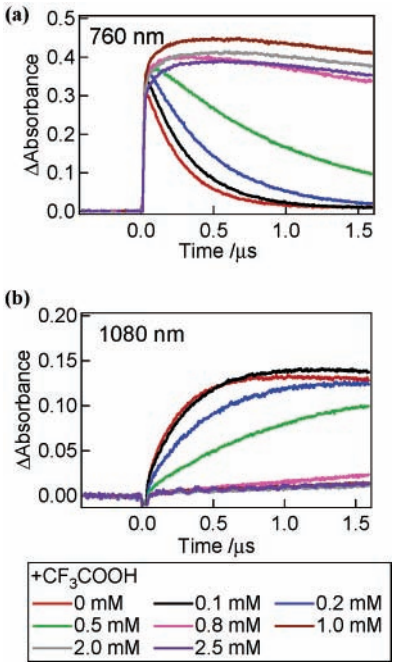

Figure 8. Changes of time profile of nanosecond transient absorption spectra of C_{60} (0.1 mM) in the presence of PS (1.0 mM) in deaerated PhCN on addition of CF_3CO_2H (a) at 760 nm and (b) at 1080 nm.

between the solvated radical ions, $(C_{60}^{\bullet-})_{solv}$ and $(PS^{\bullet+})_{solv}$, as eq 2[39−41]

$$C_{60}^{\bullet-} + PS^{\bullet+} \xrightarrow{k_{bet}} C_{60} + PS \qquad (2)$$

Since the slope of the second-order plots corresponds to $2k_{bet}/\epsilon_{ion}$, in which ϵ_{ion} refers to the molar extinction coefficients of radical ions, the k_{bet} value was evaluated to be 1.3×10^{10} M^{-1} s^{-1} in PhCN, employing $\epsilon_{ion} = 1.4 \times 10^4$ M^{-1} cm^{-1} for $C_{60}^{\bullet-}$.[10,12] In the case of *o*-DCB, similar second-order kinetics was observed for the decay of $C_{60}^{\bullet-}$, giving $k_{bet} = 2.6 \times 10^{10}$ M^{-1} s^{-1}, which is twice of that in PhCN, suggesting that the radical ions are not fully solvated in less polar *o*-DCB.[18] In toluene, on the other hand, the decay of $C_{60}^{\bullet-}$ was fast, obeying first-order kinetics, which indicates that back electron transfer takes place within the radical ion pair.[15]

Addition Effect of Acid on Time Profiles. Figure 8 shows the time profiles of $^3C_{60}$* and $C_{60}^{\bullet-}$ in the presence of PS and CF_3CO_2H; the decay rates of $^3C_{60}$* at 760 nm were slowed with the increase of $[CF_3CO_2H]$. When [PS] = 1 mM, the decay rates of $^3C_{60}$* at $[CF_3CO_2H] > 1$ mM become almost the same as without PS, suggesting that all PS changed to monoprotonated PS (PSH^+). The rise rate of $C_{60}^{\bullet-}$ also decreased with the increase of $[CF_3CO_2H]$. These observations indicate that PSH^+ does not have the donor ability to $^3C_{60}$* at all even in polar PhCN.

The $k_{first-order}$ values evaluated from Figure 8 are plotted against $[CF_3CO_2H]$ as shown in Figure 9. The observed decreasing curve is in good agreement with the decrease in the absorption band at 342 nm in Figure 2, which shows the remaining PS in the presence of CF_3CO_2H. Thus, the $k_{first-order}$ values are proportional to the remaining PS concentration.

C_{60}−PS Dyad. Optimized Structures and MO. The optimized structure of C_{60}−PS calculated by Gaussian 98 at the B3LYP/3-21G level is shown in Figure 10a. Two dimethyl groups attached to the N atoms at the 1,8-position are oriented toward opposite directions to minimize the steric crowding of the dimethylamino groups in a manner similar to pristine PS in

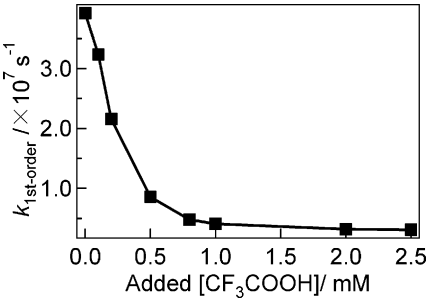

Figure 9. Plots of $k_{first-order}$ in C_{60} (0.1 mM) and PS (1.0 mM) against added $[CF_3CO_2H]$ in deaerated PhCN.

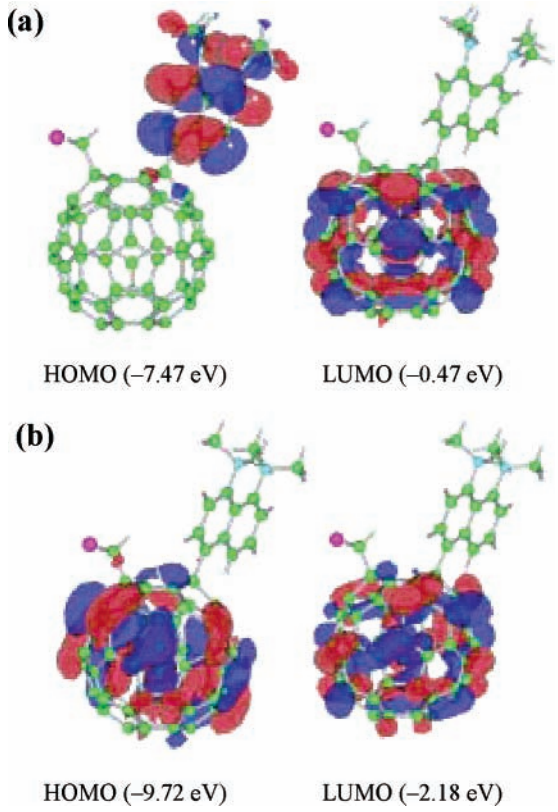

Figure 10. Optimized structure (C: green, N: blue, H: white, Cl: pink) and the HOMO and LUMO; (a) C_{60}−PS and (b) C_{60}−PSH^+.

Figure 3.[35] The HOMO is localized on the whole PS moiety, while the LUMO is localized on the whole C_{60} moiety of C_{60}−PS. This suggests that in the charge-separated state, the radical cation is localized on the PS moiety like the HOMO, which corresponds to the hole distribution.[42] On the other hand, the electron is localized on the C_{60} moiety like the electron density of the LUMO.[43]

In the presence of proton, the electron density of the HOMO shifts to the C_{60} moiety from the PSH^+ moiety as shown in Figure 10b, suggesting that the photoexcitation induces the local electronic transition within the C_{60} moiety; thus, the charge separation between the C_{60} moiety and the PSH^+ moiety is difficult.

Absorption and Fluorescence Spectra. In the C_{60}−PS dyad, the longest absorption peak of pristine C_{60} at 650 nm shifts to 690 nm by 1,4-addition; the sharp peak at 450 nm is characteristic of C_{60}-monoadducts, in which two addends are connected to C_{60} directly with two sigma bonds, losing one double bond.[44] Compared with the absorption bands of components, the broadening of the absorption bands was observed, suggesting a charge-transfer interaction in the ground state, in which the C_{60}

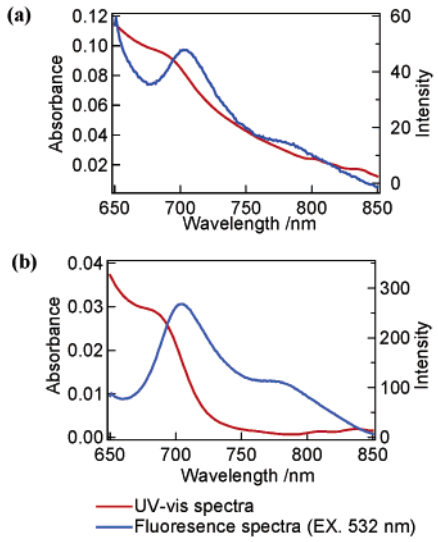

Figure 11. Absorption spectra and fluorescence spectra in PhCN; (a) C_{60}−PS (0.1 mM) and (b) C_{60}−PS (0.1 mM) and CF_3CO_2H (0.1 mM).

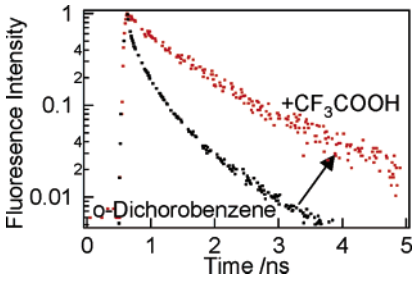

Figure 12. Fluorescence time profiles of C_{60}−PS (0.1 mM) in the absence (black) and presence (red) of CF_3CO_2H (0.1 mM) in *o*-DCB.

moiety attracts the electron cloud from the PS moiety. Figure 11a shows the absorption and fluorescence spectra of the C_{60}−PS dyad in the wavelength region longer than 650 nm. Absorption peak appeared at 690 nm, which is also characteristic of 1,4-disubstituted C_{60}.[44,45] The absorption tail extending to a longer wavelength until 850 nm may be attributed to the charge-transfer transition. The main fluorescence peak of the $^1C_{60}$* moiety of the C_{60}−PS dyad was observed at 705 nm with a Stokes shift of 200 cm^{-1}. The fluorescence wavelength region shorter than 675 nm may be attributed to the tail of the fluorescence of the PS moiety,[33] which may be excited slightly with 532-nm light at its absorption tail.

On the addition of CF_3CO_2H (Figure 11b), the absorption band at 690 nm was unchanged, while the absorption tail in the 720−850 nm region disappeared, suggesting a loss of the charge-transfer interaction by protonation of PS. The fluorescence peak also becomes sharp compared with the spectrum without CF_3CO_2H. Furthermore, the fluorescence intensity in the presence of CF_3CO_2H was greater by a factor of about 5 compared to that without CF_3CO_2H in PhCN. This suggests that the fluorescence quenching process of the $^1C_{60}$*−PS dyad in the absence of CF_3CO_2H can be attributed to charge separation yielding $C_{60}^{\bullet-}$−$PS^{\bullet+}$. However, on addition of CF_3CO_2H, such charge separation was prohibited because of the generation of C_{60}−PSH^+.

Fluorescence Lifetime Measurements. The fluorescence decay time profile of the 1,4-dialkyl C_{60} derivative showed single-exponential decay, giving the lifetime (τ_{f0}) of 1.47 ns.[45] The fluorescence time profiles of C_{60}−PS are shown in Figure 12. Without CF_3CO_2H, the fluorescence decay time profiles of C_{60}−PS showed two-component decay; the initial decay part was faster than that of reference C_{60} derivative, while slow decay rate was almost the same as that of the reference C_{60} derivative. The short fluorescence lifetimes (τ_f) were evaluated to be 0.22−0.34 ns with fraction of 50−100%, while the long lifetimes were 1.0−1.5 ns with the fraction of <50% as listed in Table 2. From the τ_f values evaluated from the predominant fast fluorescence decay parts, the rate constants (k_{CS}) and quantum yields (Φ_{CS}) of charge separation via $^1C_{60}$*−PS were evaluated using eqs 3 and 4

$$k_{CS} = (1/\tau_f - 1/\tau_{f0}) \quad (3)$$

$$\Phi_{CS} = (1/\tau_f - 1/\tau_{f0}) / (1/\tau_f) \quad (4)$$

The k_{CS} and Φ_{CS} values in *o*-DCB are larger than those in polar PhCN (Table 2). Even in toluene, charge separation takes place considerably, which is supported by the negative ΔG^0_{CS} value for charge separation via $^1C_{60}$* (Table 2).

As reasons for the slow fluorescence decay in PhCN and toluene, several factors can be considered; one is delayed fluorescence after exciplex formation[46] and another is the effect of the tail of PS fluorescence.[33]

On addition of CF_3CO_2H, the fluorescence decay rates are slowed in *o*-DCB (Figure 12) but not completely to the rate of the reference compound. The recovery of fluorescence decay rate suggests that the donor ability of the PSH^+ moiety is considerably decreased. However, since the recovery of the fluorescence decay to that of the C_{60} reference was incomplete, PSH^+ keeps a weak donor ability generating $C_{60}^{\bullet-}$−$(PSH^+)^{\bullet+}$ via $^1C_{60}$*−PSH^+. Thus, from the fast component of the τ_f values, the k_{CS} and Φ_{CS} were evaluated from eqs 3 and 4 as listed in Table 2. In *o*-DCB and toluene, the k_{CS} and Φ_{CS} values of C_{60}−PSH^+ decreased compared with those of C_{60}−PS. In PhCN, however, the opposite tendency was observed, although the recovery of the quenching of the steady-state fluorescence intensity was observed as shown in Figure 11. This observation suggests that the fluorescence decay time profiles in PhCN are quite sensitive to the impurity such as some reaction products between PhCN and CF_3CO_2H.

TABLE 2: Fluorescence Lifetimes (τ_f), Rate Constants (k_{CS}), Quantum Yields (Φ_{CS}), and Free-Energy Changes ($-\Delta G_{CS}^0$) for Charge Separation in $^1C_{60}$*−PS in Various Solvents

solvent	acid	τ_f/ns	k_{CS}/s^{-1}	Φ_{CS}	$-\Delta G_{CS}^0$/eV
PhCN		0.32 (49%)	2.4×10^9	0.76	0.79
		1.47 (51%)			
	CF_3CO_2H[a]	0.24 (78%)	3.5×10^9	0.83	
		1.26 (22%)			
o-DCB		0.22 (100%)	3.9×10^9	0.86	0.57
	CF_3CO_2H	0.55 (63%)	1.1×10^9	0.62	
		1.47 (37%)			
toluene		0.34 (76%)	2.2×10^9	0.77	0.12
		1.19 (24%)			
	CF_3CO_2H	0.51 (69%)	1.7×10^9	0.65	
		2.05 (31%)			

[a] $[CF_3CO_2H] = 0.1$ mM.

Nanosecond Transient Absorption Spectra. Transient absorption spectra observed by the excitation of the C_{60} moiety of the C_{60}−PS dyad with nanosecond laser light are shown in Figure 13a. In the absence of CF_3CO_2H, appreciable absorption bands were not observed, indicating that the lifetime of the charge-separated state ($C_{60}^{\bullet-}$−$PS^{\bullet+}$) was shorter than the laser pulse (<10 ns). On addition of CF_3CO_2H, the transient absorption bands were recovered at 670−720 nm with a shoulder at 980 nm in addition to the absorption bands at 500 and 400 nm. The main absorption peak at 700 nm was attributed to $^3C_{60}$*−PSH^+;

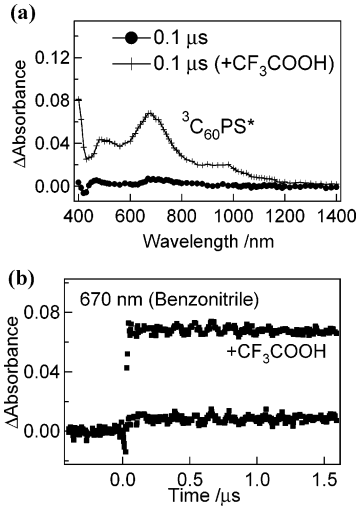

Figure 13. (a) Transient absorption spectra of C_{60}−PS (0.1 mM) in the absence and presence of CF_3CO_2H (0.1 mM) and (b) time profiles at 670 nm in the absence (red) and presence (black) of CF_3CO_2H (0.1 mM) in PhCN.

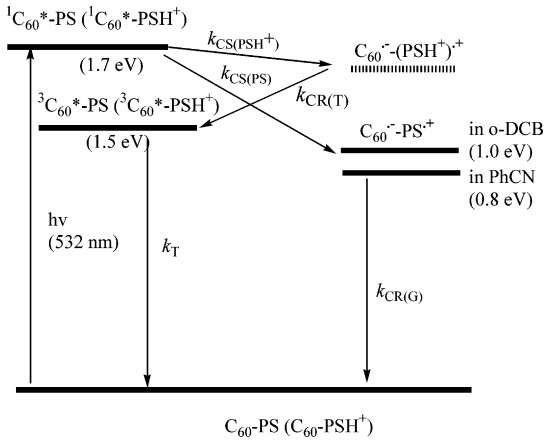

Figure 14. Schematic energy diagram for C_{60}−PS and C_{60}−PSH^+; $k_{CS(PS)}$ and $k_{CS(PSH^+)}$ are charge separation for C_{60}−PS and C_{60}−PSH^+, respectively; $k_{CR(G)}$ and $k_{CR(T)}$ are charge recombination to the ground state and triplet state, respectively.

the shoulder at 980 nm was also attributed to the $^3C_{60}$*−PSH^+. The slow decay time profile in Figure 13b in the presence of CF_3CO_2H supports the generation of $^3C_{60}$*−PSH^+. Similar transient absorption spectra and time profiles were observed in *o*-DCB and toluene, indicating the recovery of $^3C_{60}$*−PSH^+ on addition of CF_3CO_2H. Generation of $^3C_{60}$*−PSH^+ implies that charge recombination of $C_{60}^{\bullet-}$−$(PSH^+)^{\bullet+}$ generates $^3C_{60}$*−PSH^+, which has a lower energy level than that of $C_{60}^{\bullet-}$−$(PSH^+)^{\bullet+}$.

Energy Diagram. From the fluorescence peaks of the $^1C_{60}$* moiety, the energy level of the $^1C_{60}$* moiety was evaluated to be 1.7 eV, while the energy level of the $^3C_{60}$* moiety was evaluated from weak phosphorescence peak at low temperature.[47] The charge-separated states were evaluated by the Weller equation[36] using the reported electrochemical data[30] as shown in the margin under Table 1. Summarizing these data, an energy diagram can be drawn as shown in Figure 14 for C_{60}−PS and C_{60}−PSH^+. An almost similar energy diagram can be obtained for the mixture of C_{60} and PS. In the absence of acid, the energy level of $PS^{\bullet+}$ is lower than those of $^3C_{60}$*; thus, the intermolecular electron transfer is exothermic. However, on addition of acid, the energy level of $PS^{\bullet+}$ is higher than those of $^3C_{60}$*, prohibiting the electron-transfer process via $^3C_{60}$*. Although intermolecular electron transfer from PSH^+ to $^1C_{60}$* may be exothermic, a higher concentration of PSH^+ might be necessary to compete with the intersystem crossing process from $^1C_{60}$* to $^3C_{60}$*.[17]

In the case of the C_{60}−PS dyad, the energy level of $C_{60}^{\bullet-}$−$PS^{\bullet+}$ is lower than those of $^1C_{60}$*−PS and $^3C_{60}$*−PS. The charge separation takes place via $^1C_{60}$*−PS with the rate of $k_{CS(PS)}$ as fluorescence data indicate. The rapid charge recombination takes place to the ground state with the rate of $k_{CR(G)}$. On addition of acid, the energy level of $C_{60}^{\bullet-}$−$(PSH^+)^{\bullet+}$ may be higher than $^3C_{60}$*−PS but lower than $^1C_{60}$*−PS, from which charge separation is possible with the rate of $k_{CS(PSH^+)}$. Thus, after charge separation via $^1C_{60}$*−PSH^+, charge recombination generates $^3C_{60}$*−PSH^+ with the rate of $k_{CR(T)}$.

Conclusion

For C_{60}−PS mixture and C_{60}−PS dyad, photoinduced intermolecular electron-transfer process via $^3C_{60}$* and intramolecular charge-separation process via $^1C_{60}$*−PS have been confirmed by transient absorption measurements, in addition to the fluorescence lifetime measurements. In both cases, although PS works as a good electron donor, drastic changes were observed retarding these electron-transfer processes on addition of a small amount of acid. Thus, we can control effectively the electron-transfer processes by the combination of the light irradiation with a small amount of acid. We are in progress to design some acid-sensitive photoelectronic devices by applying these observations.

Acknowledgment. The present work was supported by a Grant-in-Aid on Scientific Research for the Priority Area (417) from the Ministry of Education, Science, Sports, and Culture, Japan. The authors are also grateful to Associate Professor Toshihiro Shimada of the University of Tokyo for his valuable supports.

References and Notes

(1) Mattay, J. *Topics in Current Chemistry; Photophysical and Photochemical Properties of Fullerenes*; Series 169; Springer-Verlag: Berlin, 1994.

(2) Kadish, K. M.; Ruoff, R. S. *Fullerenes*; *Chemistry, Physics, and Technology*; A John Wiley & Sons: New York, 2000.

(3) Ramamurthy, V.; Schanze, K. S. *Molecular and Supramolecular Photochemistry*; Marcel Dekker: New York, 2001; Vol. 7.

(4) Guldi, D. M.; Martín, N. *Fullerenes: From Synthesis to Optoelectronic Properties*; Kluwer Academic Publishers: The Netherlands, 2002.

(5) Echegoyen, L.; Echegoyen, L. E. *Acc. Chem. Res.* **1998**, *31*, 593.

(6) Guldi, D. M.; Prato, M. *Acc. Chem. Res.* **2000**, *33*, 695.

(7) Gust, D.; Moore, T. A.; Moore, A. L. *Acc. Chem. Rec.* **2001**, *34*, 40.

(8) Sension, J.; Szarka, A. Z.; Smith, G. R.; Hochstrasser, R. M. *Chem. Phys. Lett*. **1991**, *185*, 179.

(9) Arbogast, J. W.; Foote, C. S.; Kao, M. *J. Am. Chem. Soc.* **1992**, *114*, 2277.

(10) Biczok, L.; Linschitz, H.; Walter, R. I. *Chem. Phys. Lett*. **1992**, *195*, 339.

(11) Nonell, S.; Arbogast, J. W.; Foote, C. S. *J. Phys. Chem*. **1992**, *96*, 4169.

(12) Steren, C. A.; von Willigen, H.; Biczok, L.; Gupta, N.; Linschitz, H. *J. Phys. Chem*. **1996**, *100*, 8920.

(13) Ito, O.; Sasaki, Y.; Yoshikawa, Y.; Watanabe, A. *J. Phys. Chem*. **1995**, *99*, 9838.

(14) Ghosh, H. N.; Palit, D. K.; Sapre, A. V.; Mittal, J. P. *Chem. Phys. Lett.* **1997**, *265*, 365.

(15) Yahata, Y.; Sasaki, Y.; Fujitsuka, M.; Ito, O. *J. Photosci.* **1999**, *6*, 11.

(16) Sasaki, Y.; Ito, O.; Araki, Y.; Fujitsuka, M.; Hirao, A.; Nishizawa, H. *Photochem. Photobiol. Sci.* **2003**, *2*, 136.

(17) Sandanayaka, A. S. D.; Araki, Y.; Luo, C.; Fujitsuka, M.; Ito, O. *Bull. Chem. Soc. Jpn.* **2004**, *77*, 1313.

(18) Delgado, J. L.; de la Cruz, P.; Lo'pez-Arza, V.; Langa, F.; Kimball, D. B.; Haley, M. M.; Araki, Y.; Ito, O. *J. Org. Chem.* **2004**, *69*, 2661.

(19) Alder, R. W.; Browman, P. S.; Steele, W. R. S.; Winterman, D. R. *J. Chem. Soc., Chem. Commun.* **1968**, 723.
(20) Alder, R. W. *Chem. Rev.* **1989**, *89*, 1215.
(21) Lias, S. G.; Liebman, J. F.; Levin, R. D. *J. Phys. Chem. Ref. Data* **1984**, *2*, 814.
(22) Staab, H. A.; Saupe, T. *Angew. Chem., Int. Ed. Engl.* **1988**, *27*, 865.
(23) Williams, R. M.; Zwier, J. M.; Verhoeven, J. W. *J. Am. Chem. Soc.* **1995**, *117*, 4093.
(24) Williams, R. M.; Koeberg, M.; Lawson, J. M.; An, Y.-Z.; Rubin, Y.; Paddon-Row: M. N.; Verhoeven, J. W. *J. Org. Chem.* **1996**, *61*, 5055.
(25) Thomas, K. G.; Biju, V.; George, M. V.; Guldi, D. M.; Kamat, P. V. *J. Phys. Chem. A* **1998**, *102*, 5341.
(26) Thomas, K. G.; Biju, V.; Guldi, D. M.; Kamat, P. V.; George, M. V. *J. Phys. Chem. A* **1999**, *103*, 10755
(27) Komamine, S.; Fujitsuka, M.; Ito, O.; Moriwaki, K.; Miyata, T.; Ohno, T. *J. Phys. Chem. A* **2000**, *104*, 11497.
(28) Luo, H.; Fujitsuka, M.; Araki, Y.; Ito, O.; Padmawar, P.; Chiang, L. Y. *J. Phys. Chem. B* **2003**, *107*, 9312.
(29) Sandanayaka, A. S. D.; Matsukawa, K.; Ishi-i, T.; Mataka, S.; Araki, Y.; Ito, O. *J. Phys. Chem. B* **2004**, *108*, 19995.
(30) Lee, Y.; Kitagawa, T.; Komatsu, K. *J. Org. Chem.* **2004**, *69*, 263.
(31) Yamanaka, K.; Fujitsuka, M.; Ito, O.; Aoshima, T.; Fukushima, T.; Miyashi, T. *Bull. Chem. Soc. Jpn.* **2003**, *76*, 1341.
(32) Yamazaki, M.; Araki, Y.; Fujitsuka, M.; Ito, O. *J. Phys. Chem. A* **2000**, *104*, 11497.
(33) Szemik-Hojniak, A.; Rettig, W.; Deperasińska, I. *Chem. Phys. Lett.* **2001**, *343*, 404.
(34) Benott, R. L.; Lefebvre, D.; Fréchette, M. *Can. J. Chem.* **1986**, *65*, 996.
(35) Mallinson, R. P.; Wozniak, K.; Smith, T. G.; McCormack, L. K. *J. Am. Chem. Soc.* **1997**, *119*, 11502.
(36) Weller, A. *Z. Phys. Chem. Neue Folge* **1982**, *133*, 93.
(37) Murov, S. L.; Carmichael, I.; Hug, G. L. *Handbook of Photochemistry*, 2nd ed.; Marcel Dekker: New York, 1993.
(38) Alam, M. M.; Watanabe, A.; Ito, O. *J. Photochem. Photobiol., A* **1997**, *104*, 59.
(39) Fujitsuka, M.; Luo. C.; Ito, O.; Ito, M.; Murata, Y.; Komatsu, K. *J. Phys. Chem. A* **1999**, *103*, 7155.
(40) Sasaki, Y.; Konishi, T.; Yamazaki, M.; Fujitsuka, M.; Ito, O. *Phys. Chem. Chem. Phys.* **1999**, *1*, 229.
(41) Konishi, T.; Fujitsuka, M.; Ito, O.; Toba, Y.; Usui, Y. *J. Phys. Chem. A* **1999**, *103*, 9938.
(42) Gerson, F.; Haselbach, E.; Plattner, G. *Chem. Phys. Lett.* **1971**, *12*, 316.
(43) Frankevich, V. E.; Dashtiev, M.; Zenboi, R.; Kitagawa, T.; Lee, Y.; Murata, Y.; Yamazaki, T.; Gao, Y.; Komatsu, K.; Oliva, J. M. *Phys. Chem. Chem. Phys.* **2005**, *7*, 1036.
(44) Cheng, F.; Murata, Y.; Komatsu, K. *Org. Lett.* **2002**, *4*, 2544.
(45) Luo, H.; Araki, Y.; Fujitsuka, M.; Ito, O.; Cheng, F.; Murata, Y.; Komatsu, K. *J. Phys. Chem. B* **2004**, *108*, 11920.
(46) Kreher, D.; Hudhomme, P.; Gorgues, A.; Luo, H.; Araki, Y.; Ito, O. *Phys. Chem. Chem. Phys.* **2003**, *5*, 4583.
(47) Luo, C.; Fujitsuka, M.; Watanabe, A.; Ito, O.; Gan, L.; Huang, Y.; Huang, C. H. *J. Chem. Soc., Faraday Trans.* **1998**, *84*, 572.